29

Multifocal Multi-Photon Microscopy

Jörg Bewersdorf, Alexander Egner, and Stefan W. Hell

INTRODUCTION

Multi-photon processes relying on the cooperative action of two or more photons can broadly be divided into two families that are distinguished by the fact that the photons are either absorbed or scattered (Shen, 1984). Whereas the scattering events relevant to microscopy are second and third harmonic generation (SHG, THG), as well as coherent anti-Stokes Raman scattering (CARS), the useful multi-photon absorption events are two- and three-photon excitation (2PE, 3PE). The first multi-photon phenomenon that entered microscopy was SHG (Hellwarth and Christensen, 1974; Gannaway, 1978), followed by CARS (Duncan *et al.*, 1982), 2PE (Denk *et al.*, 1990; Curley *et al.*, 1992), 3PE (Hell *et al.*, 1996; Maiti *et al.*, 1997), and THG (Barad *et al.*, 1997; Müller *et al.*, 1998). Timed with the advent of more accessible pulsed lasers, the seminal work by Denk and colleagues (1990) on 2PE microscopy opened a new epoch of research and application with multi-photon processes in microscopy (Guo *et al.*, 1997; Gauderon *et al.*, 1998; Zumbusch *et al.*, 1999; Campagnola *et al.*, 2002; Cheng *et al.*, 2002; Müller and Schins, 2002; Yelin *et al.*, 2002; Theer *et al.*, 2003; Zipfel *et al.*, 2003).

The use of multi-photon phenomena provides several advantages over their single-photon counterparts. The most prominent is the confinement of signal generation to the focal region where the simultaneous occurrence of multiple photons is highest. Another important advantage is the capability to penetrate deeper into strongly scattering specimens (Denk and Svoboda, 1997; Centonze and White, 1998). Moreover, SHG, THG, and CARS (Zoumi *et al.*, 2002; Cox *et al.*, 2003) generate signals that are not accessible through single-photon interactions, thus complementing fluorescence imaging in a unique way.

Unfortunately, multi-photon events have a low probability of occurrence, that is, they have a small cross-section. Small cross-sections can be compensated by large excitation intensities. In microscopy, the strong focusing provided by the objective lens readily yields large intensities, in particular in conjunction with pulsed illumination. The only issue is that the applicable intensity is limited by photodamage, which also has a major nonlinear component (see Chapter 38, *this volume*). In some cases, multi-photon absorption may also reach (singlet-state) saturation. With the exception of the important application of imaging into strongly scattering tissue, the power of presently available lasers usually greatly exceeds the power required at a given point. Therefore, the use of several parallel foci may be regarded as an obvious solution to this problem. In multi-photon microscopy, this solution is particularly attractive because the optical sectioning is provided by the multi-photon interaction alone. No back-imaging onto an array of pinholes is needed, which otherwise would require delicate alignment and the compensation of chromatic aberrations. In this chapter, we give an overview of parallelized multi-photon imaging methods, which are commonly referred to as multi-focal multi-photon microscopy (MMM).

Background

Owing to their wavelength tunability, short pulse length, and high repetition rate, mode-locked titanium : sapphire (Ti : Sa) lasers have become the light sources of choice for multi-photon microscopes. Mode-locked Ti : Sa and similar laser systems typically provide 1 to 2 W of average power at a repetition rate of ~80 MHz at pulse lengths of ~200 fs or 1 to 2 ps. This is ample light for a single scanning beam since nonlinear damaging effects normally limit the usable intensity to about 200 GW/cm^2 at 200 fs and 70 GW/cm^2 at 1 to 2 ps in the focus (Hänninen *et al.*, 1995; König *et al.*, 1996, 1999; Hopt and Neher, 2001). At typical repetition rates and focal spot sizes, this maximum focal intensity amounts to 3 to 10 mW at 200 fs and 10 to 30 mW in the picosecond range average power. An important exception is the imaging of layers inside strongly scattering specimens, such as skin and brain at >250 µm depth, where most of the laser light is needed and femtosecond operation is preferable. Therefore, in regular, single-spot multi-photon microscopy, more than 90% of the laser power is discarded because applying more power would be detrimental. This holds both for the multi-photon absorption and the multi-photon scattering microscopy modes. By splitting up the beam of a mode-locked Ti : Sa laser into several beamlets and applying multiple, well-separated foci simultaneously, MMM exploits a much larger fraction of the available laser power, and at the same time it parallelizes the imaging process without significant trade-offs in the resolution (Bewersdorf *et al.*, 1998; Buist *et al.*, 1998).

Determination of the Optimum Degree of Parallelization

If photodamage, photobleaching, or saturation of an excited state of the chromophore can be neglected, the signal S from a single focus n-photon excitation microscope, per time unit, is proportional to $\sigma_S P_{avg}^n/\tau^{n-1} f^{n-1}$, with P_{avg} being the average laser power in the focus, τ and f being the pulse length in the sample and the repetition rate, respectively. σ_S is the multi-photon cross-section. In MMM, the laser beam is split up into N beamlets with an average power of $P_{avg,MMM}/N$ each. The signal of the N independent foci adds up to an overall signal $S \propto \sigma_S P_{avg,MMM}^n/(\tau f N)^{n-1}$. Within the framework of sheer signal generation, the parameters τf and N are of equal

Jörg Bewersdorf, Alexander Egner, and Stefan W. Hell • Max Planck Institute for Biophysical Chemistry, 37070 Göttingen, Germany

importance and therefore the change of one parameter can be compensated by adjusting one of the others. This can be illustrated by looking at the laser pulse train at a certain spot in the sample. The number of pulses arriving per second is proportional to f times N. Whether the repetition rate f is halved and N is doubled or vice versa is of no importance. A doubled pulse length τ can similarly be interpreted as two subsequent pulses. While τ and f are given by the laser system, the degree of parallelization N introduces a new degree of freedom to optimize the performance of a multi-photon microscope. It has to be noted though that N strongly influences the microscope design and thus can be changed only in a certain range without major technical modifications.

The choice of the parameters for MMM depends on the limiting factors: saturation, photodamage, and the available laser power. Saturation obviously does not play a role for the scattering modes because in this case no long-lived state of the sample is involved. The overall damage per time unit can be written as a polynomial series $D \propto \sum_{i=1}^{\infty} \delta_i P_{avg,MMM}^i \Big/ (\tau f N)^{i-1}$, with δ_i expressing the relative weight (including the damaging cross-sections) of the damaging mechanisms of the different orders of non-linearity. For a certain range of laser and imaging parameters P_{avg}, τ, f and N, D can be approximated by $D \propto \sigma_D P_{avg,MMM}^d / (\tau f N)^{d-1}$, where d is the effective order of non-linearity that typically is not an integer. d is close to the order of non-linearity of the dominating damaging mechanism which can change, for example, with the applied laser power P_{avg}. Similarly, σ_D is the effective damaging cross-section in this parameter range.

As a result, the performance ratio β of the signal S to the damage D is proportional to $\sigma_S/\sigma_D (P_{avg,MMM}/\tau f N)^{n-d} = \sigma_S/\sigma_D P_{peak}^{n-d}$. The goal obviously is to maximize the performance β. For this purpose, one has to distinguish between two different situations:

- $n > d$ **(the excitation process is of higher order of non-linearity than the dominating damaging process)**: Maximizing the peak power P_{peak} yields the highest value for β. Short pulses and low repetition rates are therefore favorable. Parallelization only decreases β. However, an increase of P_{peak} is only reasonable up to a value where damaging processes of higher order become significant.
- $n < d$ **(the excitation process is of lower order of non-linearity than the dominating damaging process)**: P_{peak} must be minimized to optimize β. Apart from applying long pulses and high repetition rates, parallelization is the best alternative. Moreover, by increasing the overall average power $P_{avg,MMM}$ and N simultaneously, β can be kept constant while at the same time the recorded signal per unit time S increases by a factor of N. This allows an acceleration of the imaging speed by this factor without increasing the damage. The maximum N is limited by the available laser power only as long as no low order damaging processes (such as heating) become dominant.

In the case of $n = d$, β does not depend on the peak power. Therefore, parallelization or a change in τ or f has no real influence. We note that the distance between the focal spots and the size of the scanning field additionally influence the relative weights δ_i of the damaging processes. Heating may be a problem if all of the average power is concentrated on a rather small scanning area of a few micrometers.

With regard to the damage, parallelization is only reasonable in the case of a higher degree of non-linearity d of the dominant damage process as compared to that of the excitation process ($n > d$). Another reason for the parallelization is enhanced scanning speed where parallelization is important even if $n > d$.

For the multi-photon excitation processes, the (rather rare case of) saturation is in the same way a highly nonlinear phenomenon. In this situation, a maximum acceptable saturation level can be defined with a corresponding focal average power P_{sat}. The ratio between the totally available average power $P_{avg,MMM}$ and P_{sat} gives the optimum degree of parallelization N_{opt}.

Investigations of photodamage with pulsed NIR illumination in living cells showed prevalent cell-damage mechanisms of the order of $2 < d < 2.5$ (König *et al.*, 1999; Hopt and Neher, 2001). *In vitro* photobleaching measurements have shown a power-dependence of $d \geq 3$ (Patterson and Piston, 2000). These findings make parallelization advisable especially for two-photon processes ($n = 2$) such as SHG, CARS, and 2PE. Whether parallelization is beneficial for higher-order multi-photon processes, such as THG and 3PE, depends on the dominating damage mechanism.

In the case of 2PE and a given laser system, the optimum degree of parallelization N_{opt} is estimated by considering the optimal focal laser power $P_{opt}(\tau,f)$ for given laser parameters and samples. N_{opt} is just given by $N_{opt} = P_{avg}/P_{opt}(\tau,f)$. This number is also the optimum increase in the recording speed of MMM compared to standard single-beam multi-photon microscopy. For a mode-locked femtosecond laser, the repeatedly confirmed power limit in the focus is reached at $P_{opt}(\tau \approx 200\,\text{fsec}, f \approx 80\,\text{MHz}) = 1$ to 10 mW (Hänninen *et al.*, 1995; König *et al.*, 1996, 1999; Hopt and Neher, 2001). If we assume that because of over-filling and reflection losses on average only 10% of the laser power can be transferred into the sample in a nearly diffraction-limited manner, this results in an optimum beamlet number $N_{opt} = 20$ to 100 with $P_{avg,MMM} \sim 100$ to 200 mW in the sample. The fraction of power transferred can of course be increased by slightly compromising the axial resolution of the system, in which case N_{opt} can be further enlarged significantly.

EXPERIMENTAL REALIZATION

A Multi-Focal Multi-Photon Microscopy Setup Using a Nipkow-Type Microlens Array

We now discuss a typical implementation of a MMM setup that was originally designed for 2PE fluorescence (Bewersdorf *et al.*, 1998) using a Nipkow-type arranged focal pattern for scanning the object. Adapting this type of microscope to other types of multi-photon microscopes is straightforward as a recently published setup for SHG multi-focal microscopy (Kobayashi *et al.*, 2002) shows. In the setup displayed in Figure 29.1(A), the expanded and collimated laser beam of a mode-locked Ti : Sa laser illuminates an array of microlenses (460 µm diameter, 6–12 mm focal length) etched on a fused-silica disk. The lenses are arranged in a hexagonal pattern such that the illuminating beam is split into small beams, referred to as beamlets, and focused into an array of approximately 5×5 foci of ~6 µm beam waist at the prefocusing plane (PFP). After the intermediate optics, the beamlets are directed into a conventional fluorescence microscope. The role of the intermediate optics is to ensure that the array of foci is imaged into the focal plane of the lens and that each beamlet is parallel at, and over-illuminates, the objective entrance pupil. The objective lens then produces a pattern of high-resolution foci at the sample. Figure 29.1(B) shows a recording of the 2PE fluorescence created by focusing into a dye solution. The typical number of 25 foci can be easily varied by changing the intermediate optics. The

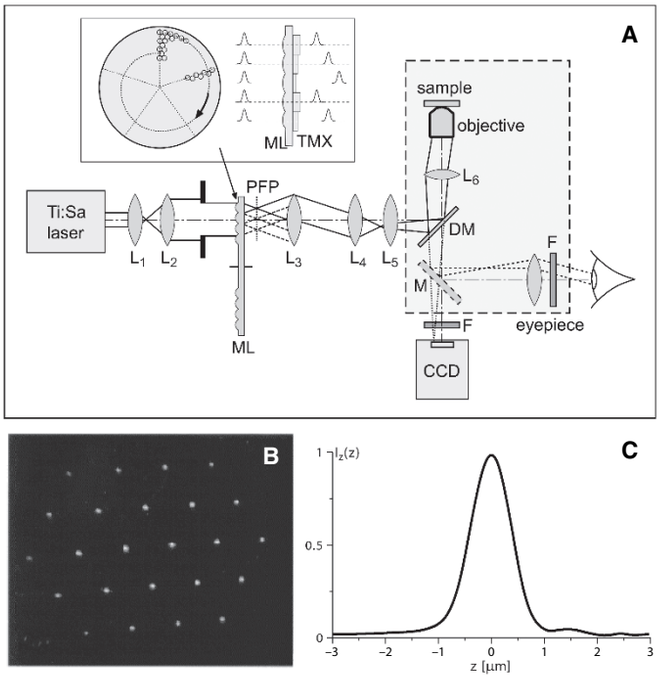

FIGURE 29.1. (A) Schematic of the first implementation of multi-focal multi-photon microscopy (MMM), including time-multiplexing (TMX). The laser beam is expanded by the lenses L_1 and L_2 and illuminates the microlens disk (ML; also shown in the inset). The microlenses focus the laser beam in the pre-focal plane (PFP), which is imaged into the sample by the lenses L_3 to L_6 and the objective lens; L_6 is the tube lens. The two-photon-excited fluorescence passes the dichroic mirror (DM) and is focused onto the CCD camera. A short-pass filter F eliminates the remaining laser light. Alternatively, by placing a mirror M into the optical detection path, the fluorescence from the focal plane in the sample can be viewed by eye. The dashed bordered box marks the parts of the conventional inverted microscope used (Leica DM-IRB). (B) The excitation pattern of the foci, recorded with the microlens disk stopped and a fluorescent solution. The experimental axial resolution of the microscope with a 1.2 NA water-immersion lens (Leica 63 × 1.2 NA water) is shown by the z-response in (C) featuring a FWHM of 890 ± 20 nm.

microlenses are arranged with a constant helical pitch [see the inset in Fig. 29.1(A)], forming spirals with typically 10 rows in a Nipkow fashion. Moreover, the layout and, in particular, the spiral pitch of the lenses are designed in such a way that the disk contains several (typically 5–12) equivalent segments. The layout of the microlenses is chosen such that upon rotation, each segment produces a complete scan of the focal area. Upon rotation of the disk, each microlens scans one line in the sample. The distance between the lines of two subsequent microlens foci in the sample remains well below the lateral resolution assuring homogeneous scanning of the sample. In the setup described the distance between the lines is 60 nm for a 100× lens. With ~500 lines per segment this results in a field of view of 35 µm diameter.[1]

In our example, the center diameter of the helix is 80 mm. The round microlenses are hexagonally closed-packed. A perfect hexagonally closed-packed plane possesses a fill factor of 90.6%. However, because of the spiral arrangement of the microlenses, the pattern is locally skewed, leading to a smaller fill factor of slightly more than 80%. The precise value slightly varies with the position on the disk. To minimize the NIR light that may pass straight to the sample causing residual out-of-focus excitation, the area between the lenses is masked. Tube lenses with different magnifications are mounted on a revolver to vary the distances between the foci in the sample and the over-illumination of the objective entrance pupil. In this way, the imaging parameters can be adapted to the specimen.

Rotating the disk by 360° renders as many complete lateral scans as segments on the disk, typically 5 to 12. The disk can be rotated at more than 100 Hz resulting in scanning rates of more than 1000 frames/s. Unlike galvanometer-based scanners, this scanning mechanism does not involve any dead time. The image rate is ultimately determined by the camera frame rate, depending on the readout rate and the number of pixels. It may range well above 30 images/s. The signal is readily separated from the NIR excitation light by a dichroic mirror and imaged directly onto a charge-coupled device (CCD) camera mounted at the microscope. With faster and more sensitive cameras, the actual limit is solely determined by the number of multi-photon–induced signal photons (fluorescence or alternatively SHG, THG, CARS, etc.) that are produced in the focal plane. Blocking the near-infrared (NIR) excitation light in the eyepieces with an absorption filter allows real-time observation of multi-photon generated images by eye. Because the excitation is restricted to the focal plane, features inside bulky objects are easily revealed.

Resolution

Because the image acquisition time is usually much slower than the scan speed, the focal plane is scanned several times during image acquisition. Mathematically, the nonlinear excitation point-spread function (PSF) $H_{exc,MMM}(x,y,z)$ of the focal pattern is integrated over the focal plane, smearing out the PSF laterally. Thus, the excitation efficiency is proportional to the z-response (Egner and Hell, 2000):

$$I_{z,exc}(z) = \int_{-\infty}^{\infty}\int_{-\infty}^{\infty} H_{exc,MMM}(x',\ y',\ z)dx'dy'. \qquad \textbf{(1)}$$

The focal plane is then imaged onto the CCD camera. This process is described by the detection PSF $H_{\mathrm{det}}(x,y,z)$, resulting in the effective PSF

$$H_{eff,MMM}(x,y,z) \propto I_{z,exc}(z)H_{\mathrm{det}}(x,y,z). \qquad \textbf{(2)}$$

This equation holds only for multi-photon absorption phenomena such as 2PE or 3PE. For scattering events, because of their coherent nature and the concomitant conservation of the phase, complex amplitude rather than intensity PSFs have to be combined in the derivation of the effective PSF. This complicates the calculation massively.

According to Eq. 2, the lateral resolution of the MMM is determined by the detection PSF in the visible wavelength range, thus, in a non-scattering specimen, it is superior to the resolution in standard non-descanned 2PE microscopy. The axial resolution, characterized by the z-response, is given by $I_{z,exc}(z)$ only, because the integral of $H_{\mathrm{det}}(x,y,z)$ across the lateral plane is of constant value. Hence we have $I_z(z) = I_{z,exc}(z)$.

The response to a homogeneously excitable half space, the so-called sea response, is a good measure for the axial imaging of an axially extended object:

[1] With a center diameter of the helical structure on the disk of ~80 mm and a microlens diameter of 460 µm, the simultaneous usage of 5 × 5 foci results in ~2500 lines scanning across the sample per revolution of the disk. For five equivalent segments, this results in ~500 lines per complete scan of the field.

$$I_{sea}(z) = \int_{-z}^{\infty} I_z(z')dz' = \int_{-z}^{\infty}\int_{-\infty}^{\infty}\int_{-\infty}^{\infty} H_{exc,MMM}(x',\ y',\ z')dx'dy'dz'. \quad \textbf{(3)}$$

Averaging a three dimensional (3D) image stack of a 2PE fluorescent solution behind a coverslip recorded with a 100× /1.4 numerical aperture (NA) oil-immersion lens, across an area several micrometers in diameter yields the sea response $I_{sea}(z)$. Figure 29.1(C) shows the experimental z-response $I_z(z)$ obtained from the derivative of the experimental $I_{sea}(z)$.

Time Multiplexing as a Solution to Interfocal Crosstalk

As with all parallelized 3D microscopes, standard MMM needs to compromise between the degree of parallelization and the crosstalk between the multiple beams. For absorption processes of the order of n, the excitation PSF of the MMM describing the distribution of the excitation efficiency in the sample at a particular instant (i.e., scanning movement neglected) is given by

$$H_{exc,MMM}(x, y, z) \propto [\tilde{h}_{ill}(x, y, z) \otimes g(x, y, z)]^{2n} \quad \textbf{(4)}$$

$\tilde{h}_{ill}$ describes the (single-focus) amplitude PSF of the illumination and the grating function g is the sum of several δ functions in the focal plane, one for each focus (Egner and Hell, 2000).

Reducing the distance between the lens foci increases the interference between the focal fields especially in the planes away from the focal plane. Because of the periodic arrangement of the lenses, the focal fields add up constructively in the so-called Talbot and fractional Talbot planes. In these out-of-focus planes, the field of different foci reinforce each other by constructive interference, yielding periodic patterns of excitation light, which results in increased out-of-focus excitation (Egner and Hell, 2000). Conventional detection with a CCD camera through a high aperture lens, images these out-of-focus-planes onto the camera where they appear mostly as a featureless background. Hence, the z-response of an MMM may differ from that of a single-beam system by an axially expanded shoulder of low amplitude [see Fig. 29.1(C) or Fig. 29.2(C)]. Problems arise if small or dim structures need to be imaged that are located in front of or behind bright voluminous objects. In this case, the shoulder may lead to a significant background signal. For a thorough discussion of this subject, including the influence of the number of foci and the distance between neighboring foci onto the z-response (Eq. 1) and the sea response (Eq. 3), we refer to Egner and Hell (2000).

Introducing a temporal delay between the beamlets solves this problem by ensuring that light pulses of neighboring foci pass the focal region at different time points (Buist *et al.*, 1998; Egner and Hell, 2000). Interference will not occur because the pulses simply do not meet each other. Hence, the excitation PSF is

$$H^{(TMX)}_{exc,MMM}(x,y,z) \propto \tilde{h}^{2n}_{ill}(x,y,z) \otimes g(x,y,z), \quad \textbf{(5)}$$

preventing the formation of Talbot planes. Apart from a constant factor denoting the number of foci, the z-response of this function does not differ from that of a single-focus multi-photon excitation PSF. Extensive calculations of different possible realizations of this time-multiplexed MMM (TMX-MMM) as well as its practical implementation have been reported (Egner and Hell, 2000; Andresen *et al.*, 2001). Using typical operation parameters (distance between foci ~4 µm, 37 foci), the use of three delay subclasses decreases the background excitation by a factor of ~3.5, whereas four subclasses decreases background excitation by a factor of ~4.5. The subclasses are chosen such that each microlens is surrounded by microlenses of the other two delay subclasses, in alternating order. For a random distribution of three subclasses, the creation of distinct Talbot planes is precluded, but the average background remains unchanged (Egner and Hell, 2000).

A realization of TMX in MMM is sketched in the inset of Figure 29.1(A). Two 300 µm thick disks with holes at the position of every third microlens (first disk) or at two of three microlenses (second disk) were glued onto the original microlens disk. The holes have the same diameter as the microlenses (460 µm) so that the microlens beamlets are divided into three subclasses: beamlets unaffected by the additional disks, beamlets delayed by ~500 fs due to one additional layer of 300 µm glass, and beamlets delayed by ~1 ps. Because of the low microlens NA (typically ~0.02), the axial focal shift induced by the additional glass is negligible. Figure 29.2 shows the comparison between the TMX-MMM and a typical Nipkow disk microscope with single-photon excitation when imaging a challenging but realistic specimen. In Figure 29.2(C), the z-profile through a 3D-image series of a fluorescent solution between two coverslips demonstrates the superior suppression of the crosstalk between the excitation foci with the TMX-MMM. This results in a much clearer representation of small details above or below bulky objects; see Figures 29.2(A,B). Although TMX has been demonstrated for 2PE only, the idea can

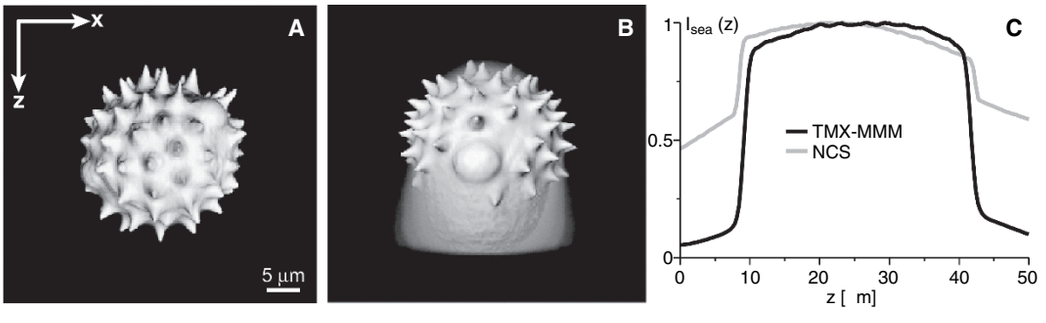

FIGURE 29.2. (A) and (B) show surfaces 3D-rendered using AMIRA Voltex of 2 grains of similar diameter (~25 µm) recorded with a 100× 1.4 NA oil-immersion lens with the TMX-MMM and a typical Nipkow confocal scanner (NCS), respectively. For a fair comparison, the parameters were selected to take the higher background of the NCS into account. Due to specimen-induced aberrations, the background behind the pollen grain in the NCS data is increased. For details see Egner and colleagues (2002). (C) The experimental sea response of a Rhodamine 6G solution of ~30 µm thickness. Note the higher background of the NCS. For example, at a distance of 5 µm away from the focal point, the background of the TMX-MMM is about seven times lower than that of the NCS.

be exploited in all multi-focal microscopy modes using pulsed or short-coherence-length illumination. It should be noted however, that for linear and multi-photon scattering events the conservation of the phase upon scattering plays a crucial role in the formation of the effective PSF.

Alternative Realizations

Besides the Nipkow-type scanning scheme, other scanning mechanisms can also be implemented. For example Buist *et al.*, (1998), use a rectangular microlens arrangement. Scanning is accomplished by rapidly moving the foci in a Lissajous pattern with an *xy* galvanometric mirror. Proper adjustment of the frequency and the amplitude of the scanning movement allows nearly uniform illumination conditions at video rate, with ~25% efficiency of light usage. MMM was also implemented in 4Pi-microscopy (Egner *et al.*, 2002b) in which case a square array of microlenses was selected. This realization was chosen because of its greater flexibility in combination with an array of detection pinholes in the focal plane of the microlenses, allowing an easy change of the pinhole size, of the focal lengths of the microlenses, as well as of the distance between the foci.

All of these setups use microlenses illuminated by an expanded and collimated laser beam to create the beamlets. To avoid wasting of the laser light, a large area of the Gaussian beam profile is used for illumination. The microlenses are much smaller than the expanded beam profile so that each individual lens is illuminated virtually uniformly. However, the microlenses in the periphery of the Gaussian profile are illuminated by less intense light than those in the center of the laser beam. This difference is carried forward to the field of view, resulting in a decrease of the intensity of the foci towards the rim. Unfortunately, the nonlinear dependence of the multi-photon process on the illumination intensity enhances this effect. If no measures are taken to homogenize this beam profile, the efficient use of the available laser power and the inhomogeneity across the field of view has to be balanced.

Masking the expanded laser beam with a rectangular aperture that blocks 70% of the laser power of a Gaussian beam, results in a ~50% decrease of the excitation efficiency at the edge of the field of view in a 2PE setup. A more constant light distribution with a better exploitation of the available laser power can be achieved by homogenizing the illumination of the microlens array. To avoid wasting large amounts of the laser light, sophisticated Gaussian-to-flat-top converters may prove useful. These use either a combination of aspheric lenses or an afocal spherical lens arrangement to redistribute the intensity to produce a homogeneous beam that also has a flat wavefront (Shafer, 1982).

Instead of dividing the expanded laser beam across its profile, the beam intensity can also be portioned by an etalon (Fittinghoff and Squier, 2000) or a cascade of beam-splitters (Fittinghoff *et al.*, 2000; Nielsen *et al.*, 2001). In this case, the beam profile is maintained for each beamlet and not relayed to the focal plane. In order to achieve the best possible resolution, the objective entrance pupil still needs to be uniformly illuminated. Dividing the beam into virtually equally intense beamlets is imperative because each beamlet illuminates a different subfield. If the ratio between the reflected and the transmitted light is not carefully chosen, discontinuous steps are obtained at the edges of the subfields in the image (e.g., a chessboard pattern). As the non-linearity n of the excitation process increases, the borders between two subfields become more noticeable. By using a high reflectivity etalon, this problem can be avoided, but a large fraction of the laser light is wasted to attain equal beamlet intensities (Fittinghoff and Squier, 2000). In addition, the tilting of the beam-splitters must be handled with particular care in order to obtain equidistant foci with each beamlet centered on the objective entrance pupil (Nielsen *et al.*, 2001).

These intensity-dividing approaches have several advantages: They are flexible, they provide a homogeneously illuminated field of view, and inherent to the beam splitting is the time multiplexing which minimizes crosstalk. Unfortunately, none of them is compatible with the spinning disk scanner. They are restricted to galvanometer or stage scanning and thus are limited in scanning speed. In addition, they involve scanning dead times.

Combining multi-focal excitation with a sample scanning setup ensures that the fluorescent light emerging from the foci is always imaged onto the same pixels of the CCD (Nielsen *et al.*, 2001). In this case, one can use the spatially resolved detection on the CCD image to remove crosstalk in the detection path between the signal emitted from adjacent foci; this may be regarded as a confocal pinhole mask by software. The approach works as long as the lateral crosstalk is limited to a region smaller than the distance between two neighboring foci.

Significant crosstalk reduction is achieved by using a pinhole array in combination with microlenses in a beam-scanning setup (Fujita *et al.*, 2000). Re-scanning of the signal across the CCD camera behind the pinholes (Egner *et al.*, 2002b) solves the problems with image acquisition encountered by Nielsen and colleagues. Detecting through pinholes slightly increases the resolution at the expense of some signal loss. For sectioning, the use of a confocal pinhole array (Fujita *et al.*, 2000) is of course not needed. However, an undeniable benefit is that the undesired scattered (fluorescence) light in multi-focal microscopy is even more suppressed.[2]

Confocalization certainly increases the contrast in the image. Unfortunately, if chromatic aberrations are not compensated, the use of pinholes always results in a significant signal loss.

The combination of MMM with a regenerative amplifier featuring a repetition rate of 1 kHz (800 nm wavelength, 110 fs pulse length) has also been demonstrated (Fujita *et al.*, 1999). To avoid severe photodamage and saturation due to the high peak powers, the setup had to be parallelized approximately 1000-fold as in a typical single-photon Nipkow confocal system (Petran *et al.*, 1968, 1985). The interfocal distance is about the same as in the systems described above. Thus, the observation of structures smaller than ~20 µm does not profit from this high degree of parallelization. Rather, the low duty cycle for each focus makes the rapid recording of small structures nearly impossible.

A commercially available version of MMM (LaVision BioTec, Bielefeld, Germany) based on an improved version of the system of Nielsen and colleagues (Nielsen *et al.*, 2001) produces a line of up to 64 foci, scanned in two dimensions by a set of galvanometer mirrors. The beam-splitter operates over the whole spectral range of the Ti : Sa laser generating foci of nearly the same intensity (difference in fluorescence ≤5%). The distance between the foci (typically 600 nm for a 60× lens) can be changed by the intermediate optics implemented. Setting the focal separation to approximately the lateral full width at half maximum (FWHM) of the PSF produces a homogeneous line of 18 µm length with high resolution. Fast scanning perpendicular to this line (up to 3.5 kHz) allows the recording of 18 µm wide rectangles of variable length, in principle, in about 0.3 ms. The recording time is currently

[2] Because in single-beam multi-photon microscopes there is no crosstalk, pinholes are reasonable only in MMM.

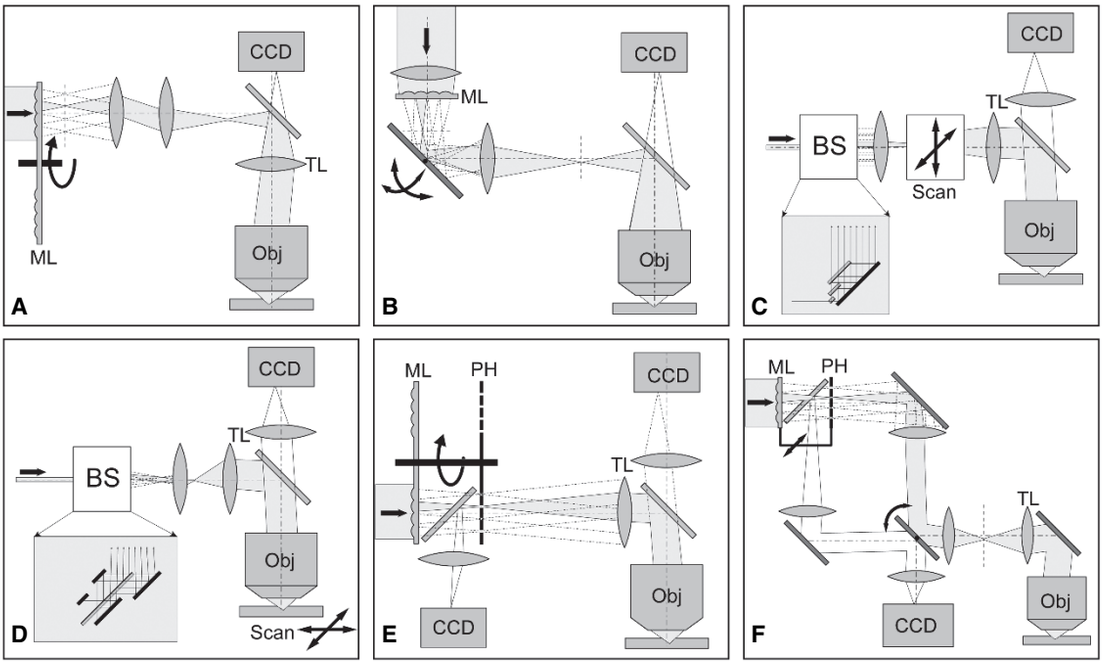

FIGURE 29.3. Different realizations of MMM. The images show sketches drawn after the original publications named, but are here simplified and rotated to ease comparison: (A) Bewersdorf and colleagues (1998), (B) Buist and colleagues (1998), (C) Fittinghoff and Squier (2000), (d) Nielsen and colleagues (2001), (E) Fujita and colleagues (2000), (F) Egner and colleagues (2002b). BS denotes the beam-splitting units of Fittinghoff, as well as of Nielsen and co-workers. Details are shown in the insets. TL, tube lens; ML, microlenses; PH, pinhole disk; Obj, objective lens.

limited by the readout speed of the camera used and the available signal. By moving the beam-splitter, the degree of parallelization can be decreased by a factor of 2. In this setup, neighboring foci are polarized perpendicular to each other allowing polarization-sensitive measurements. Figure 29.3 compares the different schemes of realizing MMM.

ADVANCED VARIANTS OF MULTI-FOCAL MULTI-PHOTON MICROSCOPY

Space Multiplexing

An option which permits improved exploitation of the total laser power and facilitates the changing of intensity levels in selected regions without attenuating the total laser power is space multiplexing (SMX) MMM (Hell and Andresen, 2001). The basic idea of SMX MMM is to modulate the intensity across the sample by the spatially modulated interference resulting from overlapping arrays of slightly offset focal fields. For a given degree of parallelization and power, SMX increases the two- and three-photon excited signal of parallelized multi-photon microscopy by a factor of up to 1.5 and 2.5, respectively. To some extent, sensitive regions may be spared, whereas in regions with weaker nonlinear susceptibilities the excitation intensity can be increased.

SMX was implemented in the MMM by splitting the collimated laser beam, combining it again with a wedge mirror and then illuminating the microlens disk. The optical path difference between the two recombined beams was changed with a piezo-driven mirror. By carefully adjusting the angle between the two beams, the interference pattern can be modified. Because the interference pattern is generated in front of the microlenses, it modulates mainly the illumination of the individual microlenses, and the influence of specimen-induced aberrations does not differ from standard MMM. As with TMX, the SMX is relevant to all modes of multi-photon microscopy, including parallelized SHG and THG imaging, CARS, and widefield multi-photon excitation.

Fluorescence Lifetime Imaging

Lifetime imaging of the fluorescent state is an important development in fluorescence microscopy. Fluorescence lifetimes are sensitive to the fluorophore environment and can be used to distinguish fluorophores with overlapping emission spectra where spectral separation is difficult. The advent of gated, intensified CCD cameras with a gate width of 200 ps and gating repetition rates of up to 100 MHz provides the opportunity of combining multifocality with lifetime imaging. Using gated cameras, lifetime images of fluorescent samples can be easily recorded with MMM (Straub and Hell, 1998a). The necessary modification includes the exchange of the standard MMM camera with a gated, intensified-CCD camera (Picostar HR, La Vision, Göttingen, Germany) and additional electronics to trigger the intensifier gate a fixed time after the excitation laser pulses. A programmable delay unit enables the recording of the fluorescence decay curves in 100 ps steps. The gate width of 200 ps and a time gap of 12.5 ns between the laser pulses, allow for the measurement of fluorophore decay times in the 0.5 to 10 ns range. Figure 29.4 shows an example of a lifetime measurement for two types of beads taken with the MMM. By using a series of time gates after each photomultiplier in a PMT array to detect all time windows instead of using a gated camera that collects signal in only a single window, the acquisition speed could be enhanced by a factor greater than 2 (see Chapter 27, *this volume*).

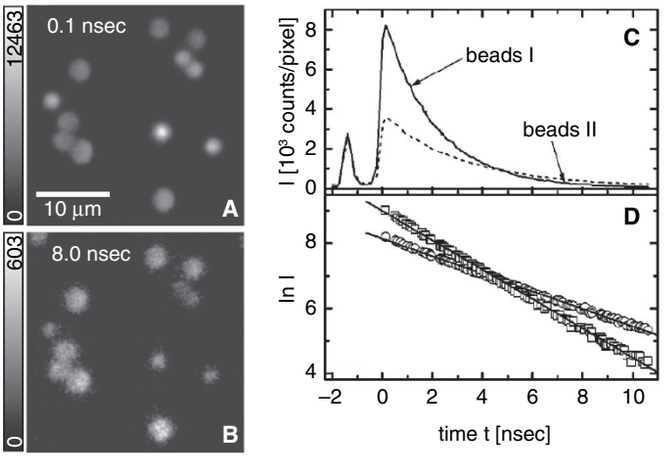

FIGURE 29.4. Fluorescence lifetime imaging with MMM. Panels (A) and (B) show images of randomly dispersed fluorescent polystyrene beads (Polysciences Inc., beads I) and larger latex beads (Molecular Probes Inc., beads II) recorded directly after the onset of fluorescence and after 8.0 ns with a gate width of 200 ps. The analysis of the decay of the fluorescence intensity *I* displayed in (C) and on a logarithmic scale in (D) yields the lifetimes of the fluorophores (2.2 and 3.7 ns for beads I and II, respectively).

Second Harmonic Generation Multi-Focal Multi-Photon Microscopy

Because SHG light is mainly forwardly scattered, the microscope is preferably used in a transmission arrangement (Kobayashi *et al.*, 2002). By modifying the MMM design, Kobayashi and co-workers imaged the focal plane with an intensified CCD camera on the far side of the sample. The sample was illuminated with a 1.2 NA water-immersion lens by applying ~100 foci with an average intensity of less than 2 mW each. By placing appropriate filters in the detection beam, the laser light ($\lambda = 896$ nm, 82 MHz repetition rate, 80 fs pulse length at the laser output) as well as light above $\lambda = 500$ nm from 2PE fluorescence was filtered out. Thereby it was possible to record multi-focal SHG images at $\lambda = 448$ nm with a typical overall exposure time between 33 ms and ~500 ms. By exchanging the detection filters, 2PE fluorescence images of the same sample can also be recorded. Kobayashi and colleagues (2002) recorded the contraction of rat cardiac myocytes with this multi-focal SHG microscope at video rate.

Multi-Focal Multi-Photon Microscopy-4Pi Microscopy

The application of MMM to 4Pi-confocal microscopy demonstrates that multiple beamlets of high optical quality can be produced. The recording times of living specimens with 4Pi-confocal microscopy can be decreased to a fraction of the rate of former setups (Egner *et al.*, 2002b, 2004).

IMAGING APPLICATIONS

MMM can be advantageously applied to the 3D imaging of biological specimens, including living cells, whenever rapid multi-photon imaging of not too-strongly-scattering specimens is needed. Pollen grains and the stem of *Prionium* stained with safranin-fast green are relatively thick, scattering test objects that have been imaged using oil-immersion lenses. Living PC12 cells stained with acridine orange, and neurons in the temporal cortex, that have been ionophoretically injected with Lucifer Yellow (Straub and Hell, 1998b) were recorded using water-immersion lenses. Nielsen and co-workers recorded 3D stacks of a CHO cell, doubly stained with ethidium bromide and fluorescein (Nielsen *et al.*, 2001). Fujita and colleagues imaged rat heart cells stained with eosin (Fujita *et al.*, 1999) as well as sections of a root of *convallaria* (Fujita *et al.*, 2000). In another study, bovine chromafin cells and NGF-differentiated PC12 cells, stained with the dyes acridin orange, FM1-43 and DiA as well as by transfection of the cells with green fluorescent protein (GFP), have been examined (Straub *et al.*, 2000). Moreover, the sectioning capability of MMM has been demonstrated in combination with 4Pi-confocal microscopy (for details see Chapter 30, *this volume*; Egner *et al.*, 2002b, 2004).

Examples of fast imaging of dynamic processes include the production of time sequences of sections through living boar sperm cells (Bewersdorf *et al.*, 1998) (Fig. 29.5), the imaging of Ca^{2+} dynamics (Fujita *et al.*, 2000), as well as a video-rate movie of the contraction of the motile microorganism *Euglena*, showing chlorophyll autofluorescence (Fittinghoff *et al.*, 2000). Using SHG-MMM, Kobayashi and colleagues recorded the contraction of rat cardiac myocytes at video rate (Kobayashi *et al.*, 2002). A study of particular biological relevance mapped Förster resonance energy transfer (FRET) using MMM to reveal important aspects of protein interaction in the Golgi apparatus in living cells (Majoul *et al.*, 2001, 2002) (see also Chapter 45, *this volume*).

An interesting application of MMM in neurobiology involved the measurement of rapid changes in free Ca^{2+} concentration over a large field of view (Cossart *et al.*, 2003). By measuring the time traces of the 2PE fluorescence of the Ca^{2+}-sensitive dye FURA2-AM simultaneously in a few hundred cell bodies in hippocampal brain slices of mice, Cossart and colleagues localized microcircuits in the neuronal network. In the example shown in Figure 29.6, they recorded time series of a single *xy*-section (443 µm × 335 µm, ~100 µm deep inside the tissue) at a rate of 150 ms/frame over 5 min with the LaVision BioTec version of the MMM and identified the cell bodies from the averaged frames [Fig. 29.6(A,B)] (Cossart *et al.*, 2005). With this information, the fluorescence time traces [Fig. 29.6(C)] corresponding to the Ca^{2+} concentration in the individual cells can be analyzed. Every dip in a time trace is interpreted as the result of an action potential. By searching for correlations in the event patterns of all the recorded cell bodies [Fig. 29.6(D)], neural microcircuits were identified [marked red in Fig. 29.6(B)]. These studies allow simultaneous measurements of the dynamic and global characterization of neuronal network activity for the first time and permit one to determine the single-cell properties of the unitary microcircuits involved in this activity.

LIMITATIONS

While it does reduce higher order photodamage effects through parallelization, MMM has its own constraints. Though normally negligible in single-beam systems (Schönle and Hell, 1998), heating of the sample may become a problem if the overall average laser power supplied to the sample is relatively large. This holds in particular for small scanning areas or if the sample contains strong single-photon absorbers.

Multifocality also leads to crosstalk arising from the reinforced overlap of the focal fields of the multiple foci. Fortunately, with the mandatory pulsed illumination, the crosstalk of the illumination light can be almost entirely eliminated by time-multiplexing every beam. The only relevant crosstalk remaining then is that

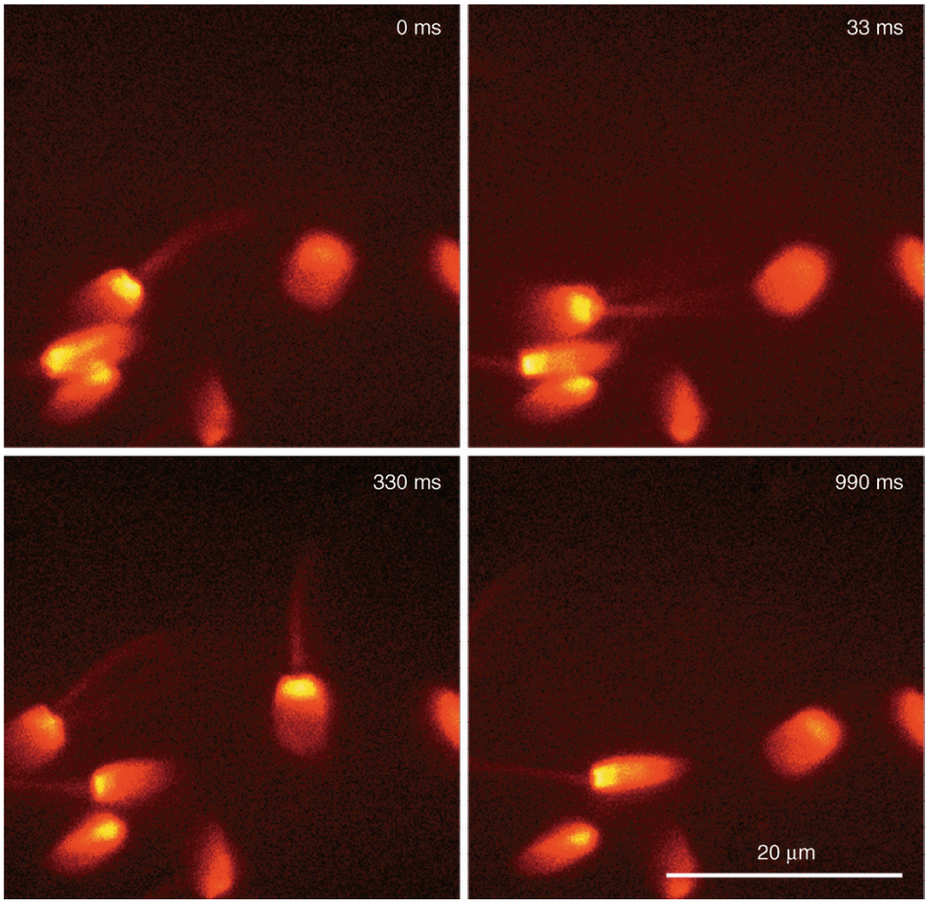

FIGURE 29.5. *xy* images of living boar-sperm cells taken with the MMM within 33 ms (30 images/s). Four typical images from a movie of 191 images are displayed. Note the movement of the sperm tail within the first 33 ms.

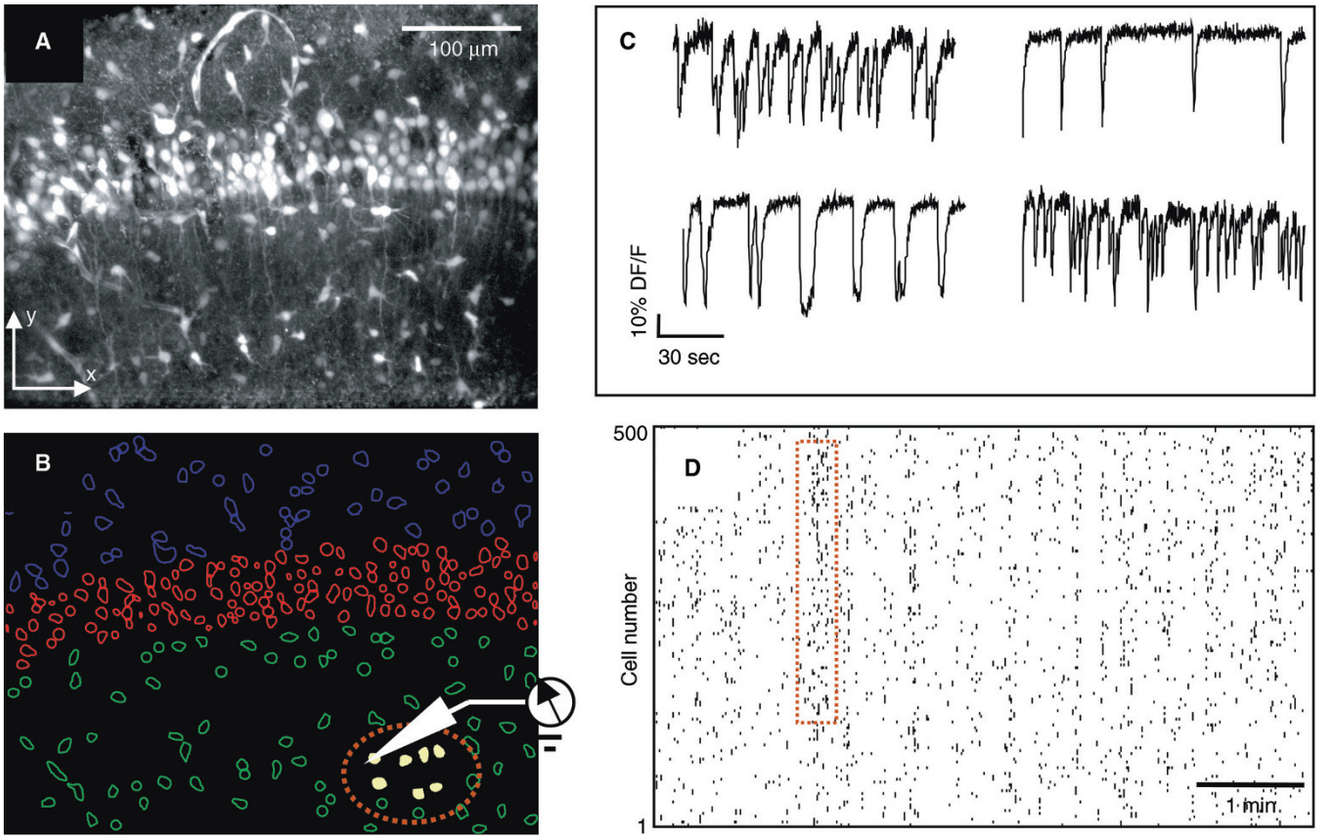

FIGURE 29.6. Identification of microcircuits in hippocampal brain slices with MMM. (A) Average of a time series of 500 consecutive frames showing the fluorescence of the Ca^{2+}-sensitive dye FURA2-AM (Olympus 20 × 0.95 NA water immersion, 150 ms/frame recording time). (B) Contours of the cell bodies automatically identified from (A). (C) Typical time traces of the fluorescence for single cell bodies taken from the time series. Each dip corresponds to an action potential causing the release of Ca^{2+} and is marked as an event in (D). (D) Rasterplot: Each horizontal line represents the time trace of a single cell. Networks are identified by correlated events (*red box*) in the rasterplot and can be visualized in the slice [*filled yellow contours* in (B)]. (Cossart *et al.*, 2005.)

which occurs because of scattering during the backimaging of the signal onto the plane of detection. However, this can be reduced by imaging the signal through an array of confocal pinholes. It also is less severe than in a conventional or in single-photon parallelized microscope, because the multi-photon–induced signal originates only at the focal plane. Figure 29.2 illustrates that the larger focal distance, the smaller number of foci, the implementation of TMX, as well as the nonlinear signal dependence in MMM leads to a crosstalk much smaller than in parallelized, single-photon confocal (Nipkow disk) microscopy (Egner *et al.*, 2002a). However, TMX could also be applied to the latter if lasers with short coherence lengths are used.

The crosstalk in the detection path and the attenuation of the intensity with deeper penetration depth may hamper the imaging of planes lying deep in strongly scattering specimens. For example, MMM is not advantageous for imaging hundreds of micrometers inside of brain tissue. Nevertheless, the success of this concept very much depends on the adaptation of the system layout to the detailed optical properties of the object. For example, one could still imagine an array of a comparatively small number of distinct foci, say 2×2, coupled to a matched array of detectors. Even without this, imaging approximately 50 µm inside of a scattering pollen grain or 100 µm inside of brain tissue is possible without major drawbacks in resolution or signal (see Figs. 29.2 and 29.6).

CURRENT DEVELOPMENTS

Of the known multi-photon imaging modes in microscopy, 2PE and SHG have already been implemented in the MMM fashion. The extension to 3PE (or even 4PE) is technically straightforward. Furthermore, the application of other multi-photon techniques to multi-focal microscopy should be uncomplicated if the microscope parameters are adjusted to the physical and biological limits of interaction cross-section and photodamage.

With the current progress in laser technology, the efficiency of MMM is expected to improve. The parallelization in MMM is not fundamentally limited by photophysical processes such as highly nonlinear damaging or bleaching or by the scanning speed. The enhancement of the efficiency in signal generation by parallelization scales directly with the increase in laser power. Thus, MMM profits directly from the new developments in laser technology. Even with the presently available lasers, a doubling of the efficiency can be achieved by combining the beams from two synchronized lasers with a polarizing beam-splitter to a single beam. Apart from a pure increase in laser power, the parameters of pulse length and repetition rate can be adapted to MMM for a more efficient operation. An increase in the repetition rate creates a better match than that between the typical 12.5 ns pulse interval of a 80 MHz laser and the 2 ns characteristic of most fluorophore decay constants, allowing a more time-efficient excitation (Bewersdorf and Hell, 1998). For samples particularly susceptible to highly nonlinear photodamage, the pulse length can be increased to reduce the peak intensity (Bewersdorf and Hell, 1998). In the opposite case, or to exploit excitation mechanisms having a higher degree of non-linearity, shorter pulse lengths can be advantageous.

A new generation of CCD cameras with on-chip amplification records with virtually no readout noise. Even though the amplification process increases the effective shot noise typically by a factor of $\sqrt{2}$ (Basden *et al.*, 2003), this allows faster imaging with frame rates at which the signal had been dominated by readout noise in the past. Alternatively, by using stage-scanning (Nielsen *et al.*, 2001), or even better, by descanning in the detection path, the CCD can also be replaced by an array of photomultipliers or avalanche photodiodes. A setup can, for example, be realized by exchanging the CCD camera in Figure 29.3(F) with a detector array and modifying the detection path so that the fluorescence light is not scanned. This alternative makes sense when imaging samples that exhibit significant scattering. By separating the foci and the concomitant detectors by a distance that is larger than the average radius of the "scattering bulb" induced by the sample, one can reduce crosstalk in the detection, while still detecting most of the fluorescence.

The design of the spinning microlens disk could easily be changed to a system that scans a line rather than a two-dimensional field. Scan rates of several thousand hertz are also in the range of resonant galvanometer scanners. However, with the spinning disk, dead times can be avoided (as long as the CCD can be read out fast enough). These features may be advantageous in physiological applications. The modification of the MMM concept to accommodate several lines at a defined distance, to a single broader line, or to other custom-defined illumination areas is also possible. Implementing microlenses with different focal lengths on the same spinning disk may be used to vary the scan plane within small dimensions as long as these are compatible with the aplanatic correction of the lens. A very interesting and promising realization of MMM implies a reduction of the lateral distance between the foci down to the size of the spot. With such an implementation scanning becomes obsolete. The result is a scanning microscope without any moving parts that, apart from the sample's linear-damage susceptibility, is limited in speed only by the pulse-repetition rate, the power of the laser, the stability of the specimen, and the readout speed of the detector (Egner and Hell, 2000; Andresen *et al.*, 2001). The realization of such a system has been demonstrated recently (Fricke and Nielsen, 2005).

For physiological applications, in which the signal of a confined illuminated region must be recorded with high temporal resolution, the MMM design can be modified so that the detection

TABLE 29.1. Advantages and Disadvantages of the Two Different Approaches of Subdividing the Beam

	Wavefront Division (Microlenses) [e.g., Fig. 29.3(A,B,E,F)]	Amplitude Division (Beam-Splitter, Etalon) [e.g., Fig. 29.3(C,D)]
Beam profile	+ Beamlet profiles close to uniform	– Each beamlet profile is a replica of the entire original laser beam profile
Homogeneity of the field of view	– Laser beam profile is transferred to field of view, resulting in lower amplitudes for outer beamlets	+ Same amplitude for all beamlets is achievable, but differences result in chessboard pattern effects
Scan speed	+ Possible use of spinning disk design allows extremely fast scan speeds >1000 frames/s	– Limited by galvanometer scanners
Handling	+ Spinning disk easy to adjust + Robust	– Adjustment more difficult + Flexible

provides no spatial resolution, for example, by using a photomultiplier tube that collects light from the illuminated area of the sample. While such a device would not provide spatial information, it would allow very fast readout of sequential data. The intrinsic 3D spatial confinement of the multi-photon–induced signal alone defines the observed volume. The illuminated region could be chosen so that signal generation is confined to a functional compartment allowing the accumulation of the signal of a larger area, increasing the sensitivity of the system. In contrast to single-beam microscopes, the shape of the illuminated region can be chosen more freely.

SUMMARY

Multi-photon microscopy complements conventional microscopy in numerous ways. However, the underlying low interaction cross-sections severely limit the resulting imaging speed and sensitivity. The use of multiple foci as practiced in MMM is an attractive solution to this problem that increases the data rate by the factor of the parallelization and avoids limitations arising from highly nonlinear damage effects or saturation. Several MMM setups have been realized, all demonstrating the various technical possibilities to parallelize multi-photon microscopy. They can broadly be divided into two groups that differ by the way they subdivide the laser beam into beamlets. Either it is the wavefront across the beam that is split into several adjacent fragments, or it is the amplitude of the laser beam that is divided into several consecutive beamlets that are eventually spread out in angle and then in space. Table 29.1 compares the advantages and disadvantages of the two approaches.

For regular imaging applications, MMM features an axial resolution that is largely uncompromised with respect to that of a single-beam scanning system. The interbeam crosstalk results in an elevated background but, in the illumination path, this can be largely avoided by time multiplexing. Due to the conservation of the phase in (nonlinear) scattering, time multiplexing is even more important for CARS, SHG, THG, etc., than for fluorescence imaging as it simply precludes non-linearly scattered light from interfering in the detection plane.

The spatial blur resulting from the transverse propagation of the non-linearly generated photons needs to be considered, but owing to the confinement of signal generation to the focal plane, this effect is significantly less pronounced than in widefield microscopy. Scattering can degrade the image quality and thus limit the maximum imaging depth. Most of the other advantages of multi-photon imaging, such as making ultraviolet (UV) illumination unnecessary for UV dyes, as well as the additional information gained from imaging modes that use nonlinear scattering, are retained.

Progress in the development of detectors and light sources will contribute to the enhancement and enlargement of the MMM family of microscopes. Additionally, new scanner and parallelization designs will further improve the performance of MMM, leading, among other things, to a fast scanning multi-photon microscopy without any moving parts.

ACKNOWLEDGMENTS

We thank R. Cossart, D. Aronov, and V. Crepel for the contribution of data about their experiments.

REFERENCES

Andresen, V., Egner, A., and Hell, S.W., 2001, Time-multiplexed multifocal multi-photon microscope, *Opt. Lett.* 26:75–77.

Barad, Y., Eisenberg, H., Horowitz, M., and Silberberg, Y., 1997, Nonlinear scanning laser microscopy by third harmonic generation, *Appl. Phys. Lett.* 70:922–924.

Basden, A.G., Haniff, C.A., and Mackay, C.D., 2003, Photon counting strategies with low-light-level CCDs, *Monthly Notices RAS* 345:985–991.

Bewersdorf, J., and Hell, S.W., 1998, Picosecond pulsed two-photon imaging with repetition rates of 200 and 400 MHz., *J. Microsc.* 191:28–38.

Bewersdorf, J., Pick, R., and Hell, S.W., 1998, Multifocal multi-photon microscopy, *Opt. Lett.* 23:655–657.

Buist, A.H., Müller, M., Squier, J., and Brakenhoff, G.J., 1998, Real time two-photon absorption microscopy using multipoint excitation, *J. Microsc.* 192:217–226.

Campagnola, P.J., Millard, A.C., Terasaki, M., Hoppe, P.E., Malone, C.J., and Mohler, W.A., 2002, Three-dimensional high-resolution second-harmonic generation imaging of endogenous structural proteins in biological tissues, *Biophys. J.* 81:493–508.

Centonze, V.E., and White, J.G., 1998, Multi-photon excitation provides optical sections from deeper within scattering specimens than confocal imaging, *Biophys. J.* 75:2015–2024.

Cheng, J.X., Jia, Y.K., Zheng, G., and Xie, X.S., 2002, Laser-scanning coherent anti-Stokes Raman scattering microscopy and applications to cell biology, *Biophys. J.* 83:502–509.

Cossart, R., Aronov, D., and Yuste, R., 2003, Attractor dynamics of network UP states in the neocortex, *Nature* 423:283–288.

Cossart, R., Ikegaya, Y., and Yuste, R., 2005, Calcuim imaging of cortical network dynamics, *Cell* 37:451–457.

Cox, G., Kable, E., Jones, A., Fraser, I., Manconi, F., and Gorrell, M.D., 2003, Three-dimensional imaging of collagen using second harmonic generation, *J. Struct. Biol.* 141:53–62.

Curley, P.F., Ferguson, A.I., White, J.G., and Amos, W.B., 1992, Applications of a femtosecond self-sustained mode-locked Ti : sapphire laser to the field of laser scanning confocal microscopy, *Opt. Quantum Electron.* 24:851–859.

Denk, W., and Svoboda, K., 1997, Photon upmanship: Why multi-photon imaging is more than a gimmick, *Neuron* 18:351–357.

Denk, W., Strickler, J.H., and Webb, W.W., 1990, Two-photon laser scanning fluorescence microscopy, *Science* 248:73–76.

Duncan, M.D., Reintjes, J., and Manuccia, T.J., 1982, Scanning coherent anti-Stokes Raman microscope, *Optics Lett.* 7:350–352.

Egner, A., and Hell, S.W., 2000, Time multiplexing and parallelization in multifocal multi-photon microscopy, *J. Opt. Soc. Am. A.* 17:1192–1201.

Egner, A., Andresen, V., and Hell, S.W., 2002a, Comparison of the axial resolution of practical Nipkow-disk confocal fluorescence microscopy with that of multifocal multi-photon microscopy: Theory and experiment, *J. Microsc.* 206:24–32.

Egner, A., Jakobs, S., and Hell, S.W., 2002b, Fast 100-nm resolution 3D-microscope reveals structural plasticity of mitochondria in live yeast, *Proc. Natl. Acad. Sci. USA* 99:3370–3375.

Egner, A., Verrier, S., Goroshkov, A., Söling, H.-D., and Hell, S.W., 2004, 4Pi-microscopy of the Golgi apparatus in live mammalian cells, *J. Struct. Biol.* 147:70–76.

Fittinghoff, D.N., and Squier, J.A., 2000, Time-decorrelated multifocal array for multi-photon microscopy and micromachining, *Opt. Lett.* 25:1213–1215.

Fittinghoff, D.N., Wiseman, P.W., and Squier, J.A., 2000, Widefield multiphoton and temporally decorrelated multifocal multi-photon microscopy, *Opt. Express* 7:273–279.

Fricke, M., and Nielsen, T., 2005, Two-dimensional imaging without scanning by multifocal multiphoton microscopy, *Appl. Opt.* 45(15):2984–2988.

Fujita, K., Nakamura, O., Kaneko, T., Kawata, S., Oyamada, M., and Takamatsu, T., 1999, Real-time imaging of two-photon-induced fluorescence with a microlens-array scanner and a regenerative amplifier, *J. Microsc.* 194:528–531.

Fujita, K., Nakamura, O., Kaneko, T., Oyamada, M., Takamatsu, T., and Kawata, S., 2000, Confocal multipoint multi-photon excitation microscope with microlens and pinhole arrays, *Opt. Commun.* 174:7–12.

Gannaway, J.N., 1978, Second-harmonic imaging in the scanning optical microscope, *Opt. Quant. Electr.* 10:435–439.

Gauderon, R., Lukins, P.B., and Sheppard, C.J.R., 1998, Three-dimensional second-harmonic generation imaging with femtosecond laser pulses, *Opt. Lett.* 23:1209–1211.

Guo, Y., Ho, P.P., Savage, H., Harris, D., Sacks, P., Schantz, S., Liu, F., Zhadin, N., and Alfano, R.R., 1997, Second-harmonic tomography of tissues, *Opt. Lett.* 22:1323–1325.

Hänninen, P.E., Schrader, M., Soini, E., and Hell, S.W., 1995, Two-photon excitation fluorescence microscopy using a semiconductor laser, *Bioimaging* 3:70–75.

Hell, S.W., and Andresen, V., 2001, Space-multiplexed multifocal nonlinear microscopy, *J. Microsc.* 202:457–463.

Hell, S.W., Bahlmann, K., Schrader, M., Soini, A., Malak, H., Gryczynski, I., and Lakowicz, J.R., 1996, Three-photon excitation in fluorescence microscopy, *J. Biomed. Opt.* 1:71–73.

Hellwarth, R., and Christensen, P., 1974, Nonlinear optical microscopic examination of structures in polycrystalline ZnSe, *Opt. Commun.* 12:318–322.

Hopt, A., and Neher, E., 2001, Highly nonlinear photodamage in two-photon fluorescence microscopy, *Biophys. J.* 2029–2036.

Kobayashi, M., Fujita, K., Kaneko, T., Takamatsu, T., Nakamura, O., and Kawata, S., 2002, Second-harmonic-generation microscope with a microlens array scanner, *Opt. Lett.* 27:1324.

König, K., Becker, T.W., Fischer, P., Riemann, I., and Halbhuber, K.-J., 1999, Pulse-length dependence of cellular response to intense near-infrared laser pulses in multi-photon microscopes, *Opt. Lett.* 24:113–115.

König, K., So, P.T.C., Mantulin, W.W., Tromberg, B.J., and Gratton, E., 1996, Two-photon excited lifetime imaging of autofluorescence in cells during UVA and NIR photostress, *J. Microsc.* 183:197–204.

Maiti, S., Shear, J.B., Williams, R.M., Zipfel, W.R., and Webb, W.W., 1997, Measuring serotonin distribution in live cells with three-photon excitation, *Science* 275:530–532.

Majoul, I., Straub, M., Duden, R., Hell, S.W., and Söling, H.D., 2002, Fluorescence resonance energy transfer analysis of protein–protein interactions in single living cells by multifocal multi-photon microscopy, *Rev. Mol. Biotechnol.* 82:267–277.

Majoul, I., Straub, M., Hell, S.W., Duden, R., and Söling, H.-D., 2001, KDEL-cargo regulates interactions between proteins involved in COPI vesicle traffic: Measurements in living cells using FRET, *Dev. Cell* 1:139–153.

Müller, M., and Schins, J.M., 2002, Imaging the thermodynamic state of lipid membranes with multiplex CARS microscopy, *J. Phys. Chem. B* 106: 3715–3723.

Müller, M., Squier, J., Wilson, K.R., and Brakenhoff, G.J., 1998, 3D microscopy of transparent objects using third-harmonic generation, *J. Microsc.* 191:266–274.

Nielsen, T., Fricke, M., Hellwig, D., and Andersen, P., 2001, High efficiency beam splitter for multifocal multi-photon microscopy, *J. Microsc.* 201:368–376.

Patterson, G.H., and Piston, D.W., 2000, Photobleaching in two-photon excitation microscopy, *Biophys. J.* 78:2159–2162.

Petran, M., Hadravsky, M., and Boyde, A., 1985, The tandem scanning reflected light microscope, *Scanning* 7:97–108.

Petran, M., Hadravsky, M., Egger, M.D., and Galambos, R., 1968, Tandem-scanning reflected-light microscope, *J. Opt. Soc. Am.* 58:661–664.

Schönle, A., and Hell, S.W., 1998, Heating by absorption in the focus of an objective lens, *Opt. Lett.* 23:325–327.

Shafer, D., 1982, Gaussian to flat-top intensity distribution lens, *Opt. Laser Technol.* 14:159–160.

Shen, Y.R., 1984, *The Principles of Nonlinear Optics*, John Wiley and Sons, New York.

Straub, M., and Hell, S.W., 1998a, Fluorescence lifetime three-dimensional microscopy with picosecond precision using a multifocal multi-photon microscope, *Appl. Phys. Lett.* 73:1769–1771.

Straub, M., and Hell, S.W., 1998b, Multifocal multi-photon microscopy: A fast and efficient tool for 3-D fluorescence imaging, *Bioimaging* 6:177–185.

Straub, M., Lodemann, P., Holroyd, P., Jahn, R., and Hell, S.W., 2000, Live cell imaging by multifocal multi-photon microscopy, *Eur. J. Cell Biol.* 79:726–734.

Theer, P., Mazahir, H.T., and Denk, W., 2003, Two-photon imaging to a depth of 1000 μm in living brains by use of a Ti:Al_2O_3 regenerative amplifier, *Opt. Lett.* 28:1022–1024.

Yelin, D., Oron, D., Korkotian, E., Segal, M., and Silberberg, Y., 2002, Third-harmonic microscopy with a titanium–sapphire laser, *Appl. Phys. B* 74(Suppl):S97–S101.

Zipfel, W.R., Williams, R.E., and Webb, W.W., 2003, Nonlinear magic: Multi-photon microscopy in the biosciences, *Nat. Biotechnol.* 21:1369–1377.

Zoumi, A., Yeh, A., and Tromberg, B.J., 2002, Imaging cells and extracellular matrix *in vivo* by using second-harmonic generation and two-photon excited fluorescence, *Proc. Natl. Acad. Sci. USA* 99:11014–11019.

Zumbusch, A., Holtom, G.R., and Xie, X.S., 1999, Three-dimensional vibrational imaging by coherent anti-Stokes Raman scattering, *Phys. Rev. Lett.* 82:4142–4145.